Numerical Simulation of Damage and Failure of a Concrete Gravity Dam Under Seismic Loads

Bi Sun *, Shan Chang, Kai Sun, Zhenyue Shi, Wenbin Lu, Yanxin He, Xiangcheng Que

Posted Date: 25 March 2026

doi: 10.20944/preprints202603.1989.v1

Keywords: earthquake; particle flow code; damage accumulation; Koyna; inertial effects

 doi:10.20944/preprints202603.1989.v1

Article

Numerical Simulation of Damage and Failure of a Concrete Gravity Dam Under Seismic Loads

Bi Sun [1,2,*], Shan Chang [1], Kai Sun [3], Zhenyue Shi [4], Wenbin Lu [5], Yanxin He [6] and Xiangcheng Que [2]

[1] Anhui Science and Technology University, Bengbu 233030, China
[2] Hohai University, Nanjing 210098, China
[3] Shanxi Ding'an Testing Co., Ltd., Taiyuan 030032, China
[4] Shandong University of Science and Technology, Taian 271019, China
[5] Henan Polytechnic University, Jiaozuo 454000, China
[6] Shandong Agricultural University, Tai'an 271018, China
* Correspondence: 11648@ahstu.edu.cn

Abstract

Since the mid-20th century, reservoir construction has increased rapidly, and the number of mega-reservoirs has risen. Consequently, the impact of earthquakes on the safety of reservoir dams has attracted growing attention. This study employed the Particle Flow Code (PFC) to conduct a dynamic damage and failure analysis of the Koyna concrete gravity dam under strong seismic loading and to investigate the influence of seismic waves and inertial effects on the dam's failure characteristics. A damage accumulation and failure index based on PFC, accounting for damage paths and the number of cracks, was proposed. When the dam was subjected to horizontal seismic waves lasting 0.82 s and vertical seismic waves lasting 0.018 s, cracks penetrated the dam. Horizontal and vertical seismic waves caused failure resulting from horizontal and vertical displacement differences, respectively. The horizontal displacement difference exhibited two peaks. The dam was more sensitive to horizontal seismic waves. The greater the inertial force, the faster the rate of damage accumulation and failure, and the greater the number of damage cracks. The inertial force of vertical seismic waves negligibly influenced the damage accumulation rate, crack initiation time, and failure mode.

Keywords: earthquake; particle flow code; damage accumulation; Koyna; inertial effects

1. Introduction

Due to rapid economic development, advances in dam engineering, and a growing demand for green energy, several state-of-the-art high concrete dams are currently under construction or are planned in western China[1]. These concrete dams are among the world's tallest and largest, and they are located in areas with complex geological and harsh environmental conditions. Under extreme loads (such as earthquakes or explosions), dam failure would not only cause massive structural losses but could also trigger severe secondary disasters[2-5]. For example, a magnitude 6.5 earthquake, several times stronger than the design peak ground acceleration, occurred in December 1967 at the Koyna Dam in India[6], resulting in cracks on the upstream and downstream surfaces of multiple non-spillway sections. A magnitude 6.1 earthquake occurred on March 19, 1962, about 1.1 km northeast of China's Xinfengjiang Dam. The strong earthquake caused an 82-meter-long through-crack at an elevation of 108 m in sections 13 to 17 of the dam. Iran's Sefid Rud headwall dam[7] was affected by a 7.3–7.7 magnitude earthquake in June 1990, which occurred 32 km from the dam toe. Through-cracks on the upstream and downstream surfaces occurred at the slope transition point in the middle of the riverbed and at construction joints; the cracks were approximately 10 mm wide and displaced downstream by about 2 cm. Therefore, researching the dynamic responses of dams under seismic loads is a critical part of disaster prevention and mitigation and vital to China's socio-

 doi:10.20944/preprints202603.1989.v1

economic development. It also represents a cutting-edge technical challenge and a major strategic issue that must be addressed in China's water conservancy projects.

Kianoush et al.[8] used the three-dimensional finite element method to analyze the seismic performance of a rectangular concrete-filled storage tank under seismic ground motion. Xu et al.[9] decomposed the self-similarity between the seismic characteristics and dynamic responses of concrete gravity dams under near-fault seismic motions and proposed a predictive model for the dam's response to near-fault seismic motions. Siva et al.[10] investigated crack propagation in the Koyna concrete gravity dam and concluded that crack propagation models were significant in dam failure simulations. Sabbagh Yazdi et al.[11] assess damage to the Koyna Dam and found that the CPU time required by the explicit Galerkin finite volume method (E-GFVM) was approximately one third that of the explicit finite element method (E-FEM). Huang et al.[12] conducted centrifuge tests and observed that dams with a frictional base exhibited the same failure mode as those with a fixed base. Haghani et al.[13] combined the extended finite element method (XFEM) with the α-method in dynamic analysis to perform time integration of shock waves following crack propagation and analyze the dynamic responses of a reservoir dam foundation during an earthquake. The α-method improved the stability of the numerical solution. Adib et al.[14] employed Abaqus to conduct nonlinear simulation analysis on the damage index of a concrete gravity dam. Sundar et al.[15] concluded through finite element simulation analysis that seismic characteristics have a significant impact on fracture morphology and failure behavior. Anari et al.[16] conducted simulation analysis on the dam-reservoir-foundation interaction system using the finite element method. Soysal et al.[17] utilized an improved finite element method to construct a discrete element framework for the nonlinear seismic behavior analysis of concrete gravity dams.

Current research on concrete gravity dams has primarily focused on numerical simulation of dam damage, failure, and crack propagation, and on computational methods. However, few studies have analyzed the effects of inertial forces. This study establishes a numerical model of a concrete gravity dam using the Particle Flow Code (PFC) to investigate dam damage and failure under seismic loads and the effects of inertial forces.

2. Design of a Concrete Gravity Dam Model

2.1. Model Sizes and Mechanical Parameters

This study focused on the Koyna gravity dam on the Koyna River in India. It has a maximum height of 103 m, a crest width of 14.8 m, and a base width of 70.2 m. It is one of the few gravity dams to have suffered damage during a major earthquake and for which complete records are available. Due to the observational data, this dam has been used as a classic case study for the dynamic analysis of concrete gravity dams. On December 11, 1967, the dam site was hit by a strong magnitude 6.5 earthquake with horizontal peak acceleration of 0.47 g and vertical peak acceleration of 0.31 g. The Koyna Dam sustained severe damage. Horizontal cracking occurred on the upstream and downstream faces of multiple non-spillway sections at the slope transition point. Seepage took place at the downstream toe of these sections, indicating that cracks had penetrated both the upstream and downstream faces, leading to through-crack failure. Many researchers[18-21] have conducted simulation analyses of the dynamic failure of the Koyna gravity dam during the Koyna earthquake. This study performed a granular flow numerical simulation of the dam to assess the influence of inertial effects on its dynamic responses. The model of the Koyna concrete gravity dam is shown in Figure 1.

 doi:10.20944/preprints202603.1989.v1

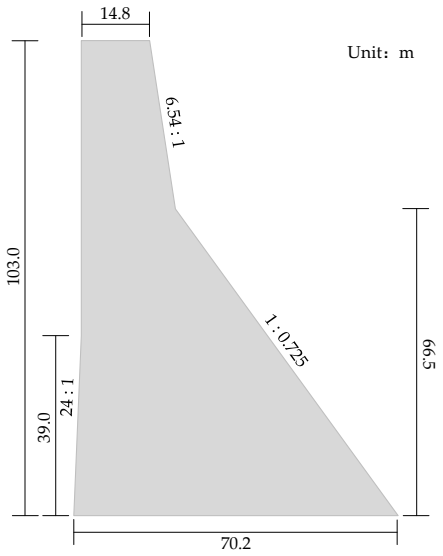

Figure 1. Profile of the Koyna gravity dam.

The material parameters for the Koyna dam are an elastic modulus of 31 GPa, a Poisson's ratio of 0.2, a density of 2640 kg/m³, a tensile strength of 2.90 MPa, and a compressive strength of 24.1 MPa. Uniaxial compression and uniaxial tensile tests were conducted before calibrating the dam's microstructural parameters. The model dimensions were 50 mm × 100 mm, with a minimum particle size of 0.3 mm and a particle size ratio of 0.45. Control variables were used. The dam's elastic modulus was 31 GPa, the mesoscale strength ratio was 2.7, and the mesoscale tensile strength was 4.23 MPa. Due to significant differences between the dam's tensile and compressive strengths, uniaxial compression specimens undergo tensile failure, and the strength is very low when the mesoscale tensile strength is low in the PFC. The ratio of mesoscale shear strength to mesoscale tensile strength is typically set to 1.2 for calibrating mesoscale strength parameters [22]. Due to the low tensile strength, the ratio of micro-shear strength to micro-tensile strength was set to 1.5 to prevent an influence on the specimen's failure mode. Consequently, the micro-shear strength was 6.34 MPa. The stress-strain curve is shown in Figure 2. The PFC uniaxial test results showed that the specimen's compressive strength was 12.27 MPa, and the tensile strength was 2.90 MPa.

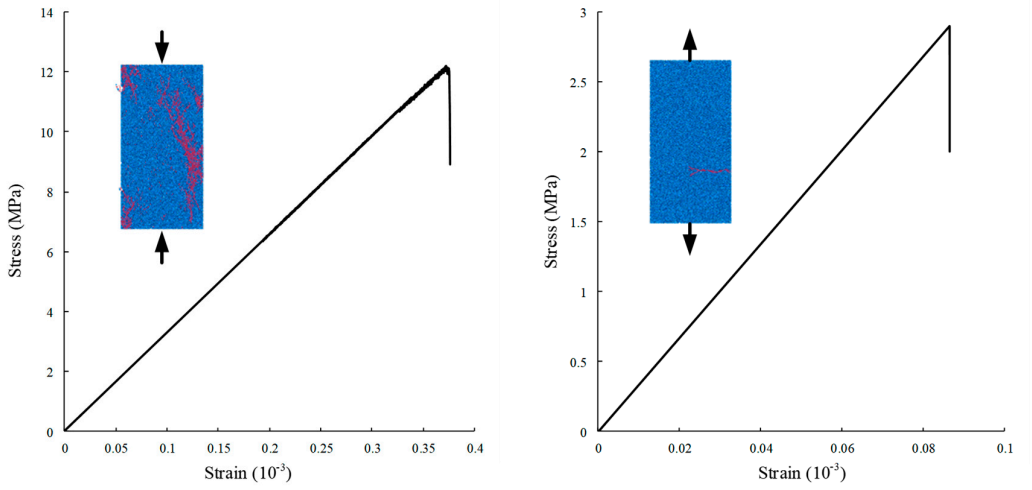

(**a**) (**b**)

Figure 2. PFC uniaxial test results: (**a**) Uniaxial compressive stress-strain curve; (**b**) Uniaxial tensile stress-strain curve.

 doi:10.20944/preprints202603.1989.v1

A force load was applied at the bottom of the model to simulate the effects of seismic acceleration on the dam. The particle radius was fixed at 100 mm to ensure uniform acceleration of the bottom particles and to reduce the computational load associated with varying particle radii. The particles at the downstream slope of the Koyna Dam model, where tensile stress concentration was more likely, were refined. The particle distribution of the dam is shown in Figure 3. The particle size ratio was 1.5, and the model generated 133380 particles.

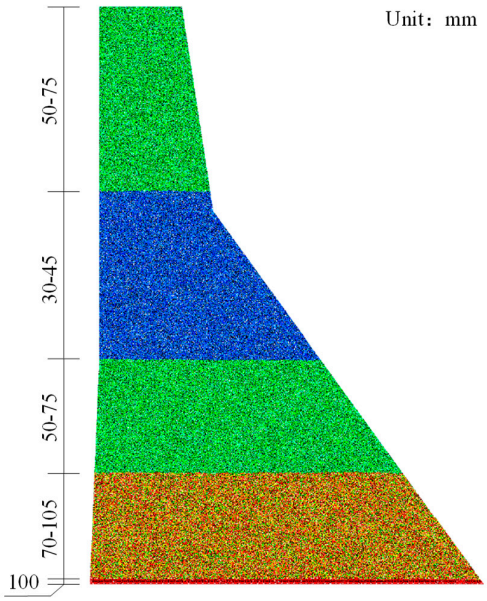

Figure 3. Particle size distribution of the numerical model of the Koyna gravity dam.

2.2. Waveform Parameters

The measured ground motion waveforms during the Koyna earthquake are shown in Figure 4. Figure 4(a) shows the horizontal acceleration waveform, and Figure 4(b) shows the vertical acceleration waveform.

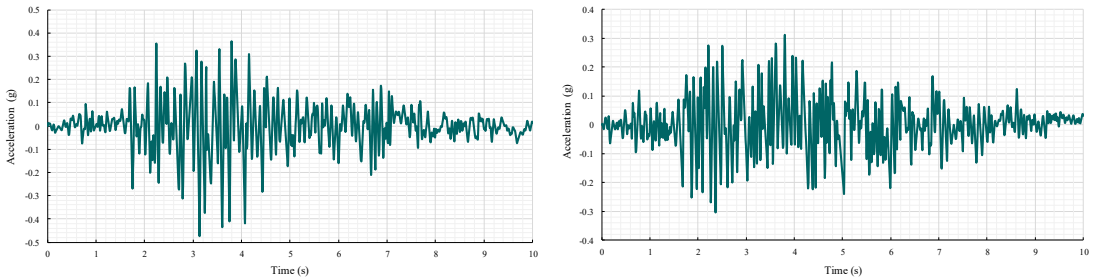

(**a**) (**b**)

Figure 4. Acceleration records of the Koyna seismic event: (**a**) Horizontal direction; (**b**) Vertical direction.

The results show that the absolute maximum amplitudes of the horizontal and vertical seismic waves are 0.474 g and 0.312 g, respectively. Both point upstream.

3. Dynamic Failure of Concrete Gravity Dams

3.1. Damage Accumulation and Failure Criteria

 doi:10.20944/preprints202603.1989.v1

In a nonlinear damage plasticity analysis, the damage factor and the extent of the damage zone characterize the degree and scope of stiffness degradation in the dam under loading, respectively. Concrete damage plasticity models can be used to analyze crack initiation, propagation, and ultimate failure in large-volume concrete structures. However, it remains challenging to use the results for a quantitative evaluation of a dam's seismic safety. This study proposed cumulative damage indices for local and global dam damage using the PFC to quantify the impact of seismic motion on the cumulative damage of concrete gravity dams. A schematic diagram of the cracking path in the dam is shown in Figure 5.

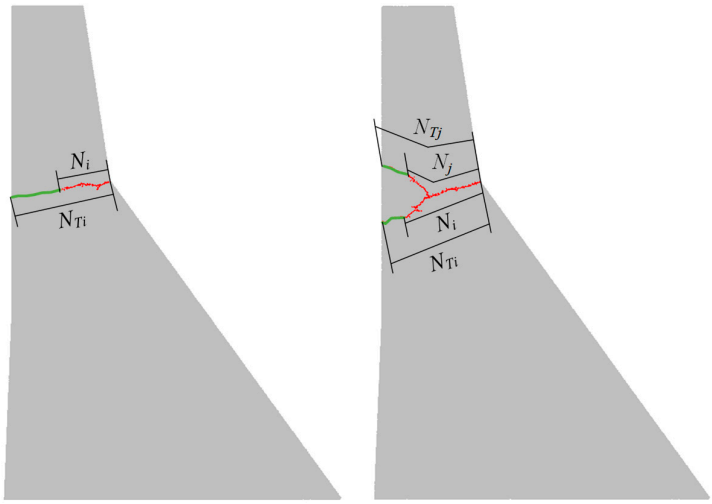

(**a**) (**b**)

Figure 5. Schematic diagram of the dam crack path: (**a**) Single crack path; (**b**) Multiple crack paths.

Figure 5(a) is a schematic diagram of a dam with a single crack path; its damage and failure criteria can be expressed as:

$$D_{dam} = \frac{N_i}{N_{Ti}} \tag{1}$$

where D_{dam} is the dam damage index; N_i is the number of cracks along crack path *i*; N_{Ti} is the total number of cracks along all possible paths of crack path *i*.

For multiple damage paths, as shown in Figure 5(b), the damage path with the longest horizontal projection was selected to calculate the cumulative damage index. Since the horizontal projections of the various damage paths are similar, this study calculated the cumulative damage index by counting the number of cracks along each path as follows:

$$D_{dam} = \max\left\{\frac{N_i}{N_{Ti}}, \frac{N_j}{N_{Tj}}\right\} \tag{2}$$

where N_j is the number of cracks along crack path *j*; N_{Tj} is the total number of cracks along all possible paths of crack path *j*.

3.2. Crack Propagation Under Horizontal Seismic Loading

Figure 6 shows the damage accumulation over time following horizontal seismic loading.

 doi:10.20944/preprints202603.1989.v1

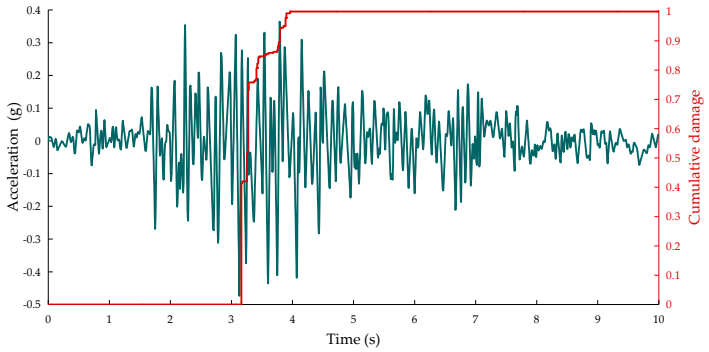

Figure 6. Damage accumulation over time under horizontal seismic loading.

Cracks appeared in the Koyna gravity dam at 3.16 s, coinciding with the peak amplitude of the seismic wave, which was pointed upstream. As the seismic wave continued to affect the dam, the cracks propagated rapidly. The cumulative damage reached 0.76 at 3.3 s, and the dam was breached at 3.98 s, resulting in complete failure that occurred at 0.82 s.

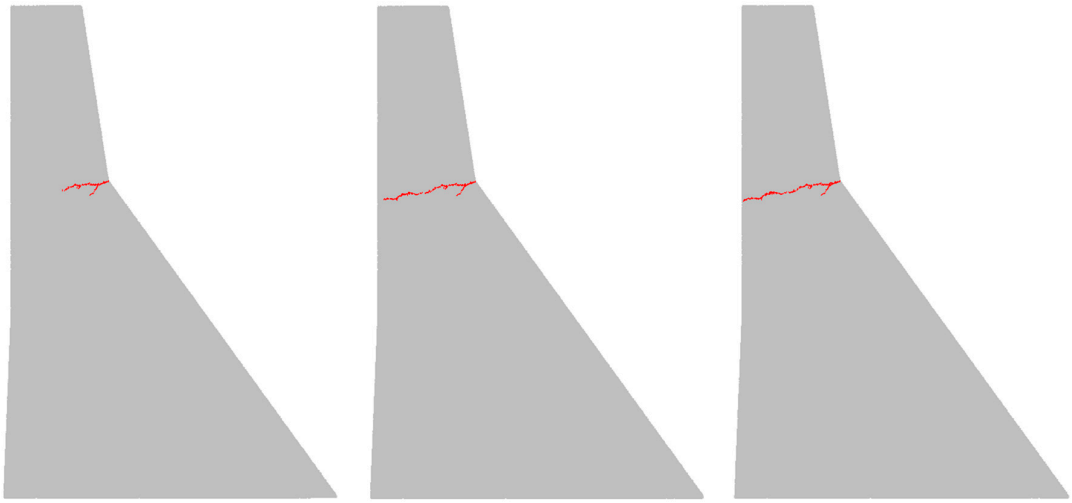

(**a**) (**b**) (**c**)

Figure 7. Crack propagation and damage of the dam during an earthquake.: (**a**) 3.2 s; (**b**) 3.3 s; (c) 3.6 s.

This study focused on the period from 3.2 s to 3.6 s, during which most crack propagation and significant dynamic responses occurred, as shown in Figure 7. At 3.2 s (Figure 7(a)), cracking and failure occurred at the downstream slope of the dam, primarily due to high tensile stress concentrations. Subsequently, the crack propagated diagonally into the dam body. Since the stress at the crack tip included tensile stress caused by the dam's bending, shear stress induced by inertial forces in the upstream direction, and compressive stress caused by the dam's self-weight, the crack did not propagate horizontally upstream but bent downward (Figure 7(b)). At 3.6 s (Figure 7(c)), the downstream crack had nearly penetrated the upstream face. The dam failure mode obtained from this simulation was consistent with the results for the Koyna gravity dam reported in the literature[20], indicating that the computational method was valid.

3.3. Evolution of the Contact Force Chain Under Horizontal Seismic Loading

This study examined changes in the contact forces of the dam under horizontal seismic loading from the Koyna earthquake. The distribution of the contact force chain at different times is shown in Figure 8.

 doi:10.20944/preprints202603.1989.v1

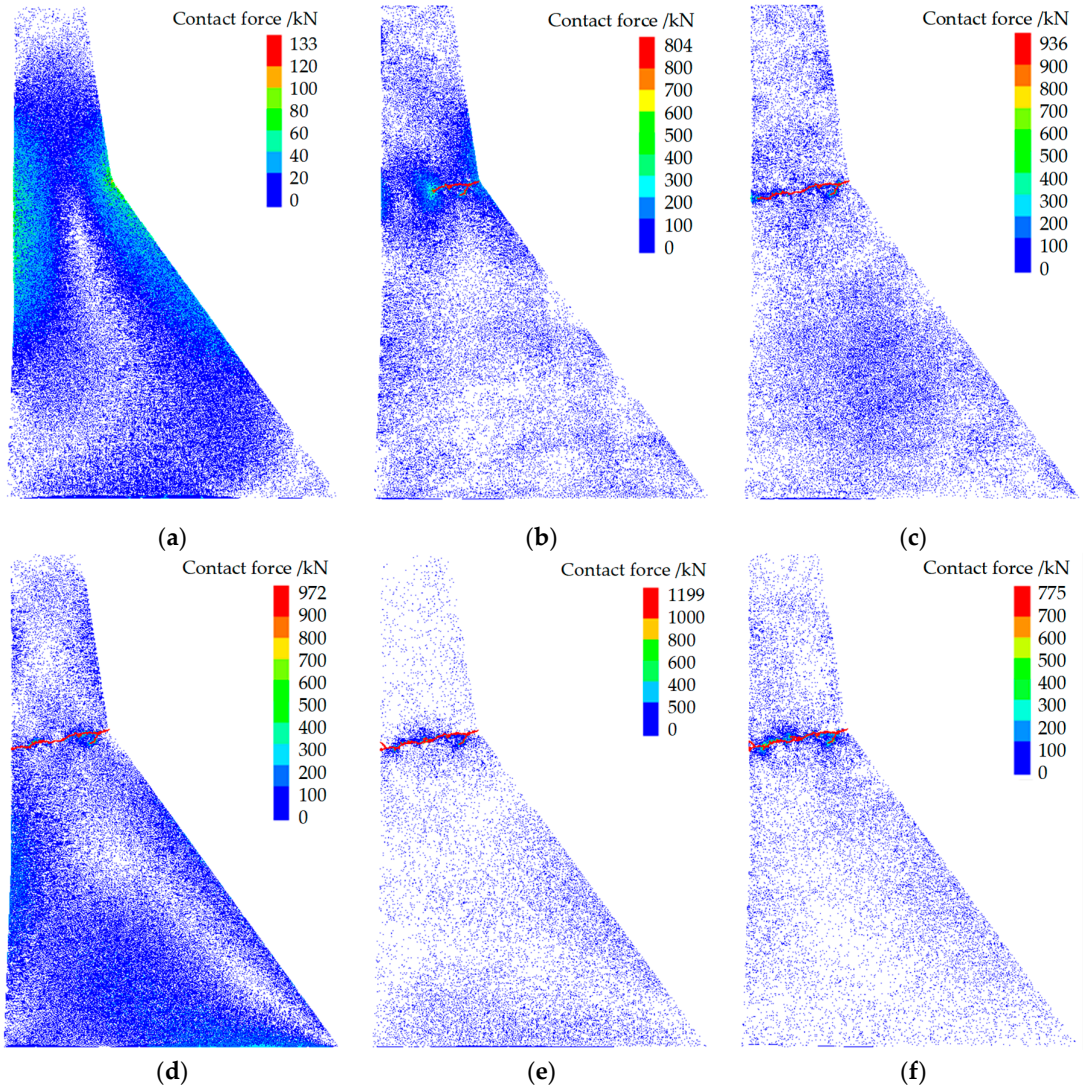

Figure 8. Evolution of the contact force chain: (**a**) 1.0 s; (**b**) 3.2 s; (c) 3.3 s; (**d**) 3.6 s; (**e**) 4.0 s; (f) 10.0 s.

After 1.0 s of horizontal seismic loading (Figure 8(a)), stress concentrations appeared on both the upstream and downstream faces at the slope transition point. After 3.2 s (Figure 8(b)), cracks formed on the downstream face at the slope transition point, with stress primarily concentrated at the crack tips and on the upstream and downstream faces. The stress was slightly lower on the downstream face, and the stress magnitude continued to increase. After 3.3 s of loading (Figure 8(c)), the crack continued to propagate diagonally into the dam body. Stress concentration remained concentrated at the crack tip, and its magnitude continued to increase. After 3.6 s of loading (Figure 8(d)), the crack penetrated the entire dam. The contact force reached its maximum value of 972 kN. It was primarily concentrated at the crack inflection point and the tips of the branching cracks. During loading from 4.0 s to 10.0 s (Figure 8(e–f)), the contact chain and stress magnitude remained unchanged.

3.4. Evolution of Horizontal Displacement

The evolution of horizontal displacement in the Koyna gravity dam during loading is shown in Figure 9.

 doi:10.20944/preprints202603.1989.v1

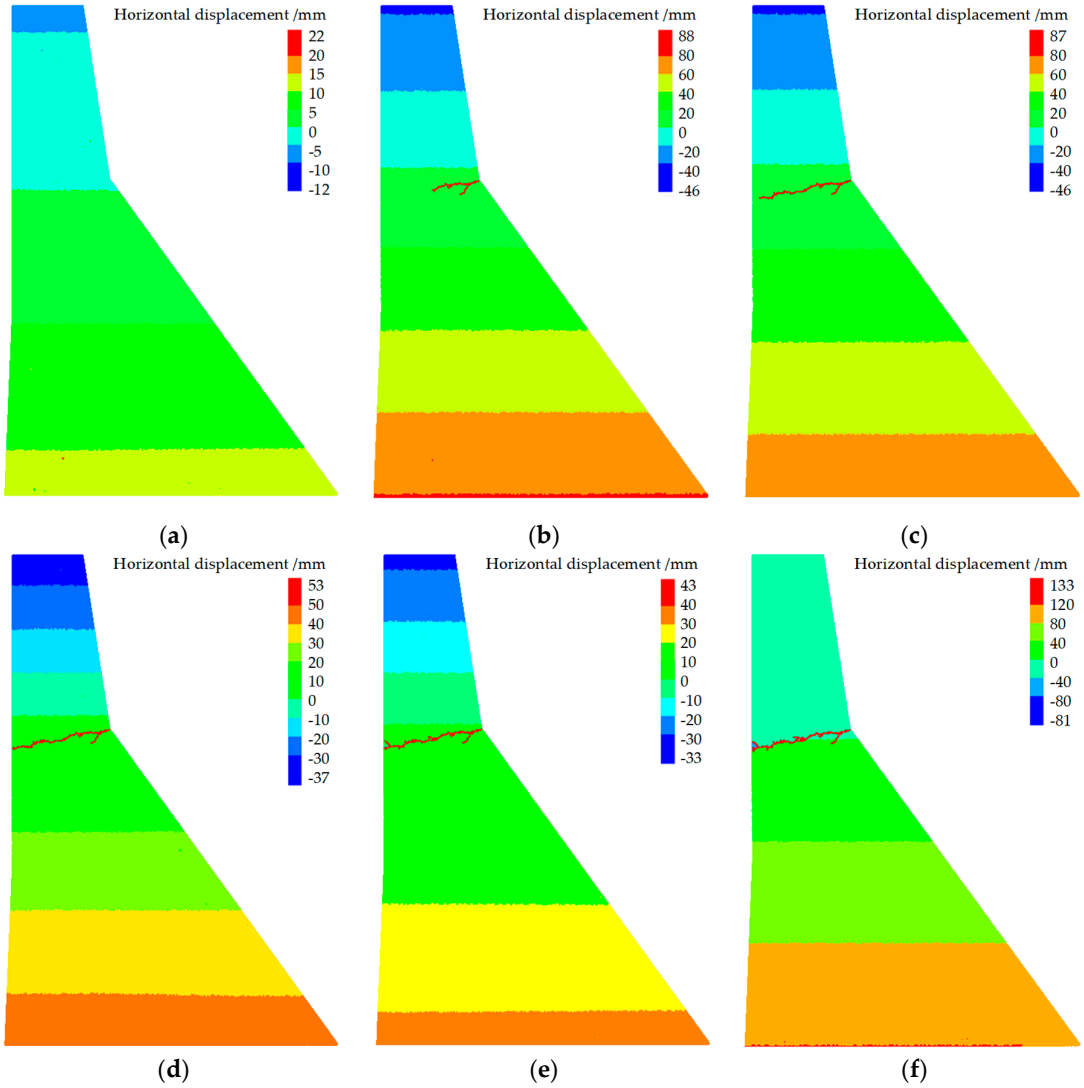

Figure 9. Evolution of horizontal displacement: (**a**) 1.0 s; (**b**) 3.2 s; (c) 3.3 s; (**d**) 3.6 s; (**e**) 4.0 s; (f) 10.0 s.

Figure 9 shows contour plots of the dam's horizontal displacement at different time intervals. After 1.0 s of loading (Figure 9(a)), the horizontal displacement occurred in layers. The absolute displacement was large and pointed downstream at the dam foundation, whereas it was small and directed upstream at the dam crest. At 3.2 s (Figure 9(b)), the layering became more pronounced. The asynchronous displacement between the dam's crest and foundation was caused by inertial forces. The displacement difference between the two locations eventually led to the dam failing, resulting in a crack at the downstream slope transition. At 3.3 s (Figure 9(c)), the crack had nearly penetrated the entire dam, and the displacement of the dam foundation remained high. At 3.6 s (Figure 9(d)), the crack had propagated through the entire dam, whereas the displacement of the dam foundation had decreased significantly. The displacement of the dam foundation increased from 0 s to 10.0 s (Figure 9(e–f)), with the displacement of the upper half of the fractured dam increasing from bottom to top. The reason is that the displacement directions of the dam foundation and the dam crest were opposite. After the through-crack had formed, friction at the fracture plane pushed the particles near the upper fracture zone in the opposite direction (downstream), reducing their displacement and resulting in a relatively larger displacement at the dam crest.

Figure 10 shows the displacements at the dam's crest and toe at different times and their differences.

 doi:10.20944/preprints202603.1989.v1

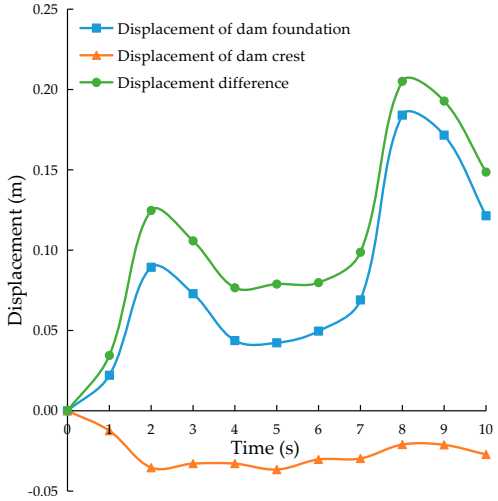

Figure 10. Displacements at the dam's crest and foundation and their differences.

As shown in Figure 10, the variation in displacement at the dam crest was relatively small (0.03 m) from 2.0 s to 10.0 s. Therefore, the displacement difference curve closely resembled the displacement trend at the dam foundation, which exhibited two peaks. The first peak occurred at 2.0 s. No cracks had formed, but significant shear forces existed. As shown in Figure 8, the shear forces were primarily located on the upstream and downstream faces corresponding to the dam's slope transition zone. The second peak occurred at 8.0 s. Cracks had completely penetrated the dam, and the displacement of the dam foundation was less constrained by the fractured upper portion, resulting in greater displacement.

3.5. Crack Propagation Under Vertical Seismic Loading

Figure 11 shows the damage accumulation over time following vertical seismic wave loading.

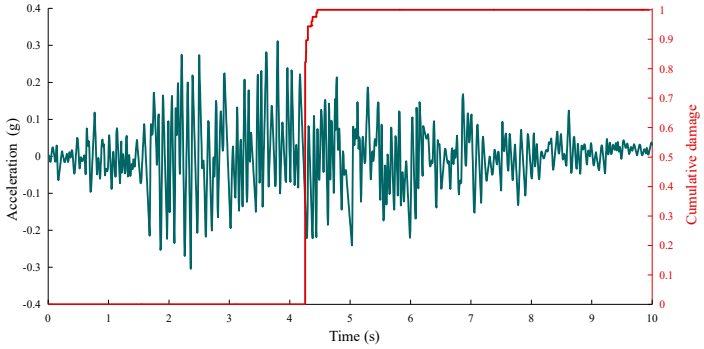

Figure 11. Damage accumulation over time under vertical seismic loading.

Damage cracks appeared in the Koyna gravity dam at 4.259 s. The cumulative damage reached 0.9 rapidly. At 4.277 s, cracks had almost penetrated the dam, with cumulative damage reaching 1.0 during 0.018 s.

 doi:10.20944/preprints202603.1989.v1

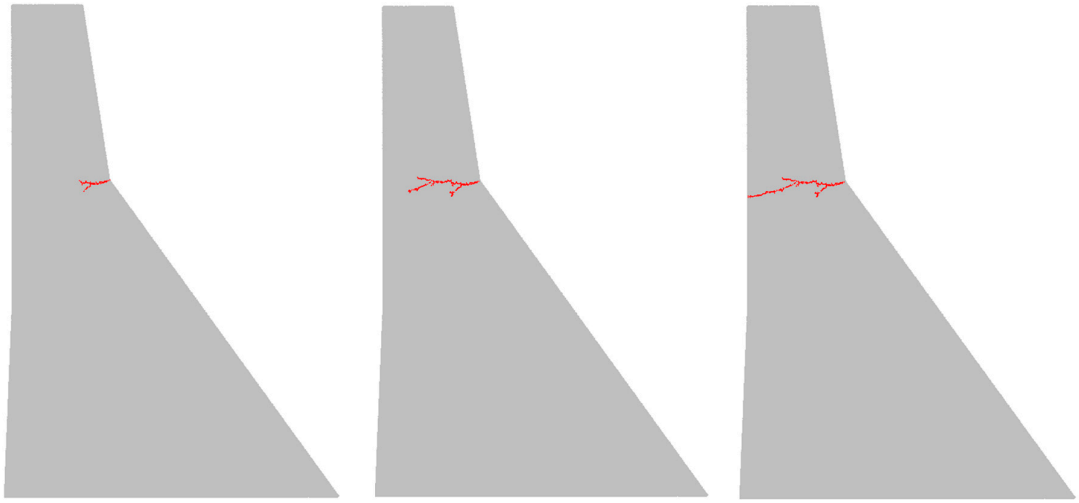

(**a**) (**b**) (**c**)

Figure 12. Crack propagation and damage to the dam: (**a**) 4.26 s; (**b**) 4.265 s; (c) 4.277 s.

The analysis focused on the period from 4.26 s to 4.277 s, which was the critical stage of crack propagation and significant dynamic responses, as shown in Figure 12. At 4.26 s (Figure 12(a)), a crack propagated and caused failure at the downstream slope of the dam, primarily due to high tensile stress concentrations. Subsequently, the crack propagated diagonally and downward toward the dam body. By 4.265 s (Figure 12(b)), the crack had penetrated two-thirds of the dam. At 4.277 s (Figure 12(c)), the downstream crack had penetrated the upstream face, resulting in through-crack failure.

3.6. Evolution of the Contact Force Chain Under Vertical Seismic Loading

The evolution of the contact force chain of the Koyna Dam under vertical seismic loading is shown in Figure 13.

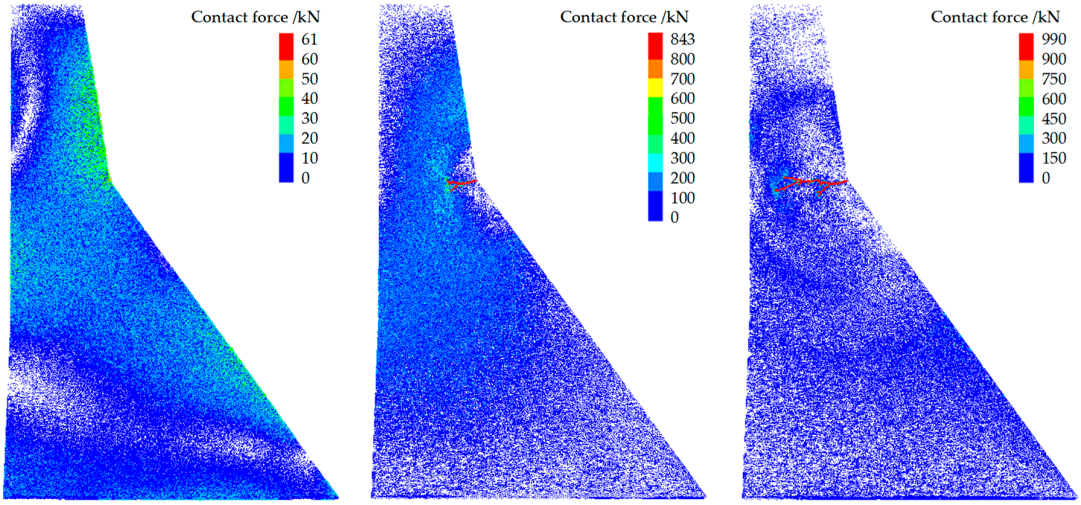

(**a**) (**b**) (**c**)

 doi:10.20944/preprints202603.1989.v1

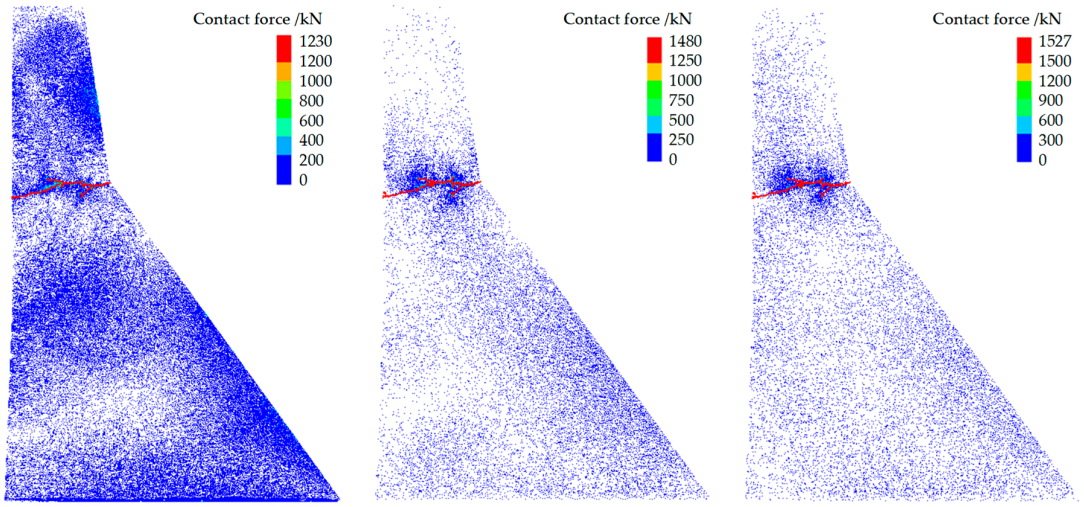

Figure 13. Evolution of the contact force chain: (**a**) 1.0 s; (**b**) 4.26 s; (c) 4.265 s; (**d**) 4.277 s; (**e**) 6.0 s; (f) 10.0 s.

After 1.0 s of vertical seismic loading (Figure 13(a)), stress concentrations appeared on both the upstream and downstream faces of the dam's slope. They were located lower on the upstream face, and the force chains were concentrated along the inclined surfaces. At 4.26 s (Figure 13(b)), cracks formed on the downstream face at the slope transition point. The stress was concentrated at the crack tips, and the curve had an S-shape. At 4.265 s (Figure 13(c)), an oblique crack propagated into the dam rapidly, with stress still concentrated at the crack tips, and the contact force continued to increase. After 4.277 s of loading (Figure 13(d)), the crack penetrated the entire dam, with a maximum contact force of 990 kN. It was primarily concentrated at the crack inflection point and the tips of the branching cracks. The contact force remained constant at around 1500 kN from 6 s to 10 s (Figure 13(e–f)), and the number of cracks did not increase.

3.7. Evolution of Vertical Displacement

The evolution of the dam's vertical displacement over time is shown in Figure 14.

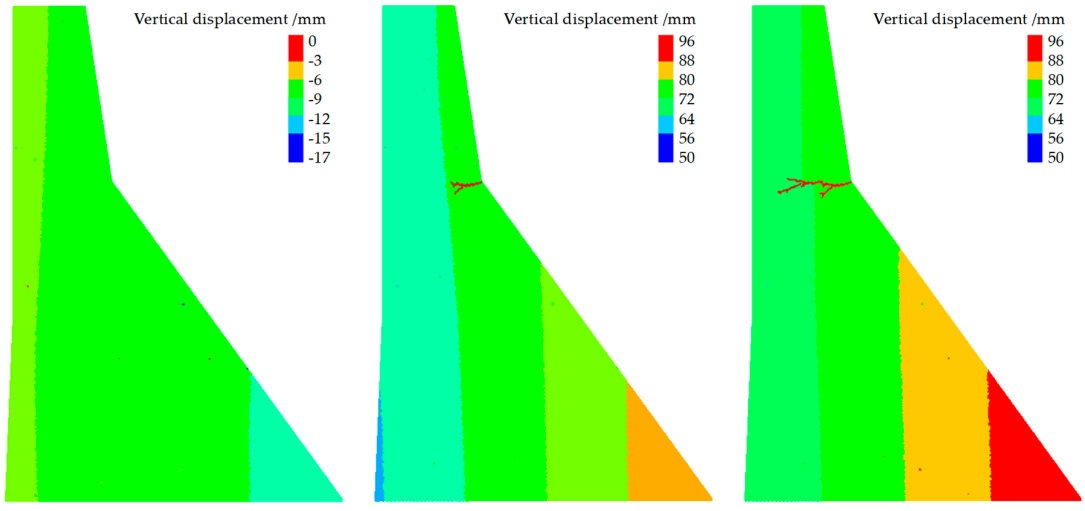

 doi:10.20944/preprints202603.1989.v1

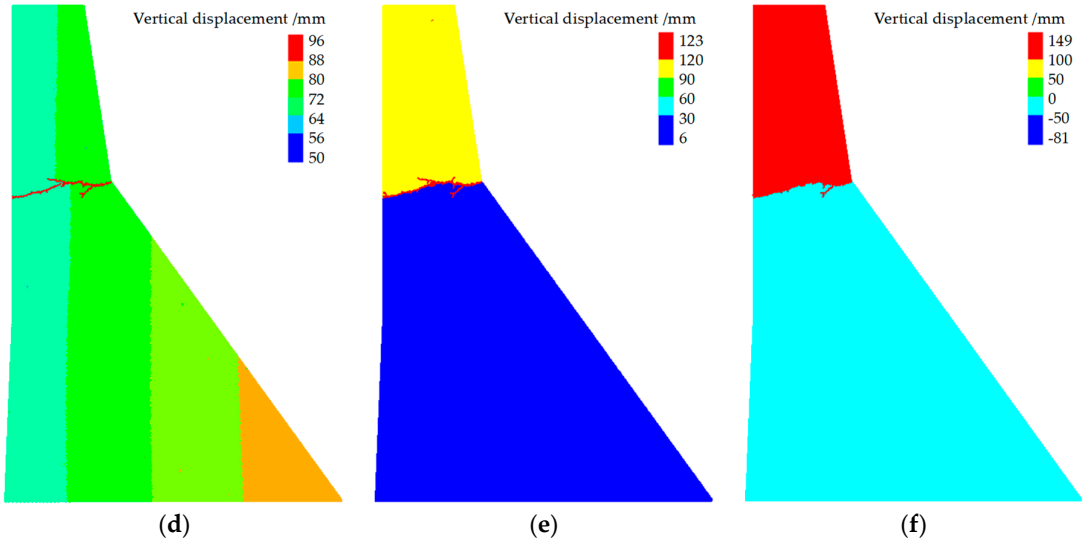

Figure 14. Evolution of vertical displacement: (**a**) 1.0 s; (**b**) 4.26 s; (c) 4.265 s; (**d**) 4.277 s; (**e**) 6.0 s; (f) 10.0 s.

After 1.0 s of loading (Figure 14(a)), a layered pattern was observed in the horizontal displacement of the dam's upstream and downstream faces. The displacement increased from the upstream face to the downstream face, resulting in a vertical displacement difference. At 4.26 s (Figure 14(b)), the dam could no longer withstand the unbalanced vertical forces, causing cracks to form at the downstream slope transition. From 4.265 to 4.277 s (Figure 14(c–d)), the cracks propagated and penetrated the entire dam, while the magnitude of vertical displacement remained nearly constant. At 6.0 s (Figure 14(e)), the dam's displacements were inconsistent. The upper half had completely detached from the dam body, and the displacement magnitude had increased. By 10.0 s (Figure 14(f)), the displacement of the dam body increased slightly, whereas the displacements of the upper and lower fractured sections were greater.

In summary, the horizontal and vertical seismic waves passing through the dam lasted 0.82 s and 0.018 s, respectively, resulting in cracks that c penetrated the dam. All cracks originated at the break in the slope on the downstream face and extended diagonally downward to the upstream face. The horizontal seismic wave caused a horizontal displacement difference in the dam, leading to its failure, whereas the vertical seismic wave generated a vertical displacement difference, resulting in cracks in the dam and the dam's failure.

4. Inertial Effects

Under dynamic loading, interactions between rock particles and the soil result in acceleration. On a macroscopic scale, the bearing capacity exhibits a nonlinear trend, which is known as the inertial effect. It substantially influences the dynamic response and failure modes of gravity dams under seismic loads. During an earthquake, the inertial forces generated by the dam's mass significantly alter the stress distribution, affecting crack initiation, propagation paths, and the final failure mode. A systematic analysis of the inertial effects on the evolution of dam damage and failure modes was conducted by assessing seismic waveforms with different characteristics under horizontal and vertical loading. The results provide a comprehensive theoretical basis for the seismic design and safety assessment of gravity dams.

4.1. Loading Waveform Design

Velocity pulse and force pulse waves produce identical loading effects[23, 24]. However, since force loading enables better control of acceleration, this study used this approach. During force loading, controlling the amplitude and rise time of a trapezoidal waveform does not accurately describe the influence of inertial effects on the model. Therefore, waveforms with different rise times

 doi:10.20944/preprints202603.1989.v1

were used to investigate the impact of inertial effects on gravity dams. The horizontal and vertical loading waveforms are shown in Figure 15.

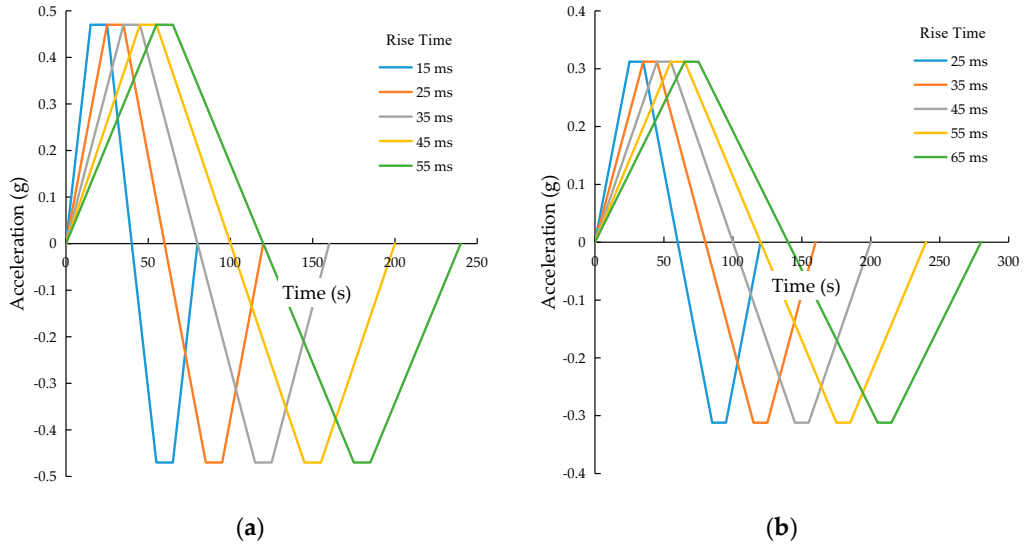

Figure 15. Loading waveforms in two directions: (**a**) Horizontal direction; (**b**) Vertical direction.

4.2. Horizontal Loading

A horizontal seismic wave (Figure 15(a)) was applied to the dam, with each waveform lasting three times its period. The cumulative damage to the dam is shown in Figure 16.

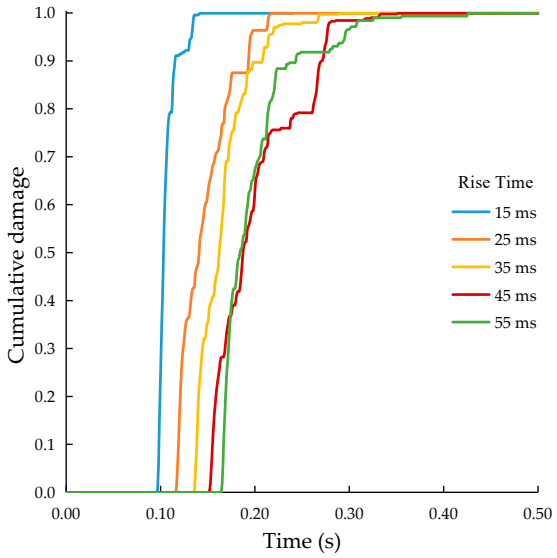

Figure 16. Cumulative damage curve of the dam under horizontal loading with different waveforms.

The shorter the rise time of the loading waveform, i.e., the steeper the slope of the waveform, the faster the rate of damage accumulation. For example, at a rise time of 15 ms, the cumulative damage to the dam increased rapidly to 0.9. Conversely, as the rise time increased, the rate of damage accumulation slowed, and the time when cracking started was delayed. Therefore, the greater the horizontal seismic inertial force, the faster the damage accumulation and the earlier the cracking and failure time.

Figure 17 shows the damage and failure patterns of the dam under different loading waveforms.

 doi:10.20944/preprints202603.1989.v1

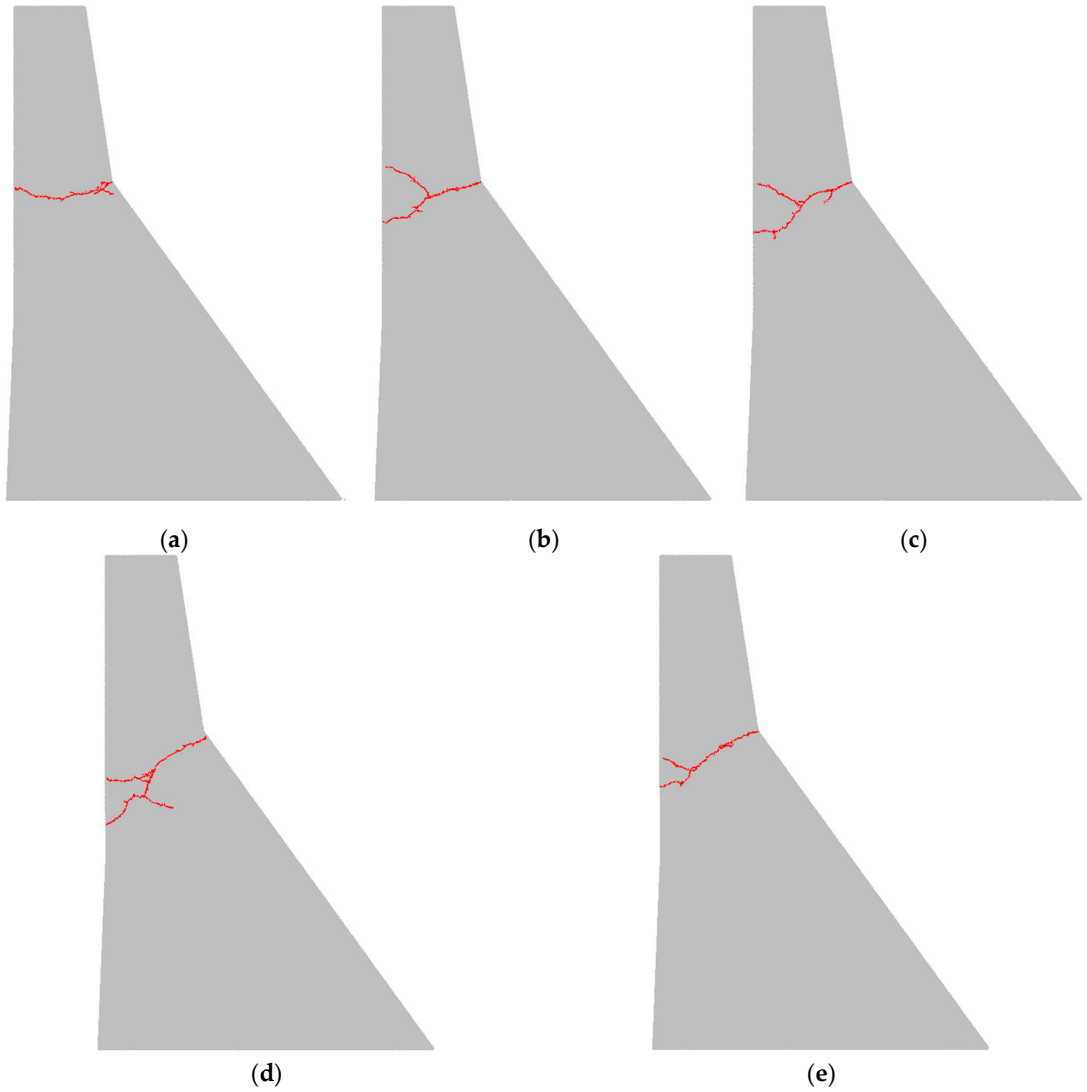

Figure 17. Damage and failure modes of dams with different rise times: (**a**) 15 ms; (**b**) 25 ms; (**c**) 35 ms; (**d**) 45 ms; (**e**) 55 ms.

Under different loading waveforms, cracks formed on the downstream face at the slope transition point and propagated diagonally downward into the dam until they reached the upstream face, penetrating the entire dam. Only a single crack occurred at a rise time of 15 ms (Figure 17(a)). The reason is the short rise time of the loading waveform and the high rate of damage accumulation, which caused the crack to penetrate the dam rapidly. However, at rise times of 25–55 ms (Figure 17(b–e)), the failure patterns were similar. Therefore, the horizontal seismic inertial forces significantly affected the dam's failure mode. The smaller the inertial force, the more damage cracks appeared.

4.3. Vertical Loading

Figure 15(b) shows the cumulative damage to the dam under vertical loading with different waveforms, which lasted three times the period.

 doi:10.20944/preprints202603.1989.v1

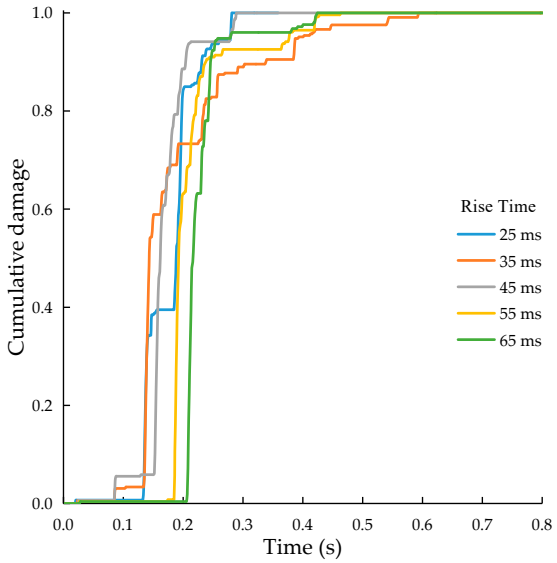

Figure 18. Cumulative damage curve of the dam under vertical loading with different waveforms.

As shown in Figure 18, the rise time had a negligible effect on the rate of damage accumulation or the time of crack initiation, indicating that vertical inertial forces had a minor impact on damage accumulation.

The effect of different loading waveforms on the damage and failure modes of the dam is shown in Figure 19.

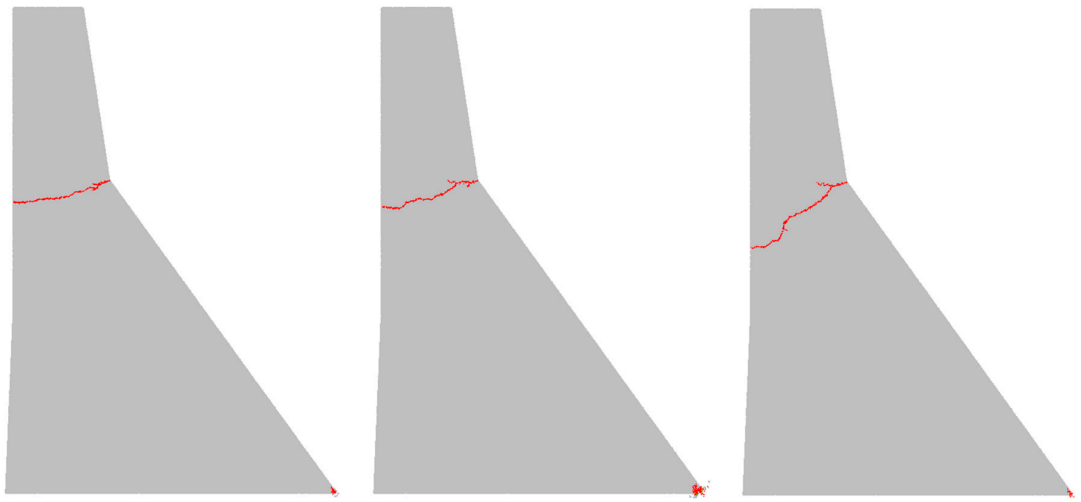

(**a**) (**b**) (**c**)

 doi:10.20944/preprints202603.1989.v1

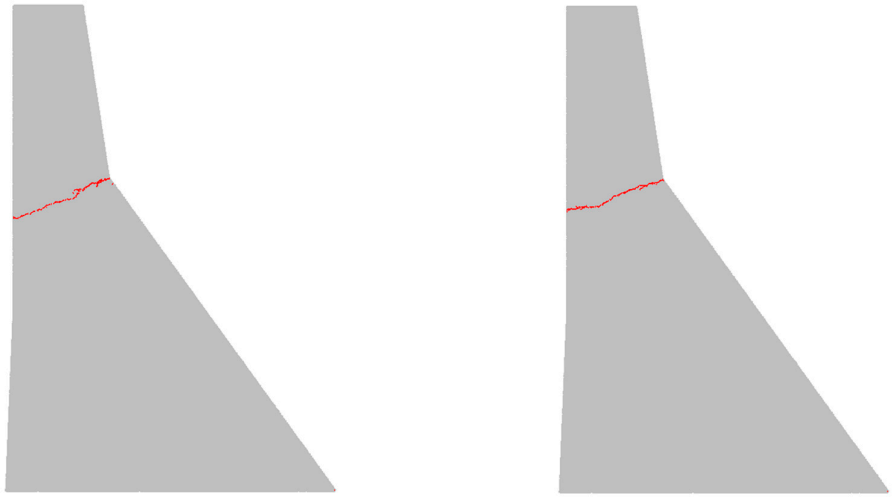

(**d**) (**e**)

Figure 19. Damage and failure modes of the dam for different rise times: (**a**) 25 ms; (**b**) 35 ms; (**c**) 45 ms; (**d**) 55 ms; (**e**) 65 ms.

Under different loading waveforms, cracks in the dam originated from the downstream face at the slope transition point and propagated diagonally downward into the dam until they reached the upstream face, penetrating the entire dam. The failure modes were similar for loading waveforms with different rise times. Single inclined cracks with no significant branching were observed. They propagated diagonally downward from the downstream toe of the slope until they penetrated the dam. Therefore, the inertial forces perpendicular to the seismic wave had a minor influence on the dam's failure mode.

5. Conclusions

The dynamic failure behavior of dams under seismic loads is a cutting-edge, critical technical issue and an important strategic challenge in hydraulic engineering. This study conducted a dynamic damage and failure analysis of the Koyna concrete gravity dam under strong seismic loads using PFC to investigate the influence of seismic waves and inertial effects on the failure characteristics of gravity dams. The following conclusions were reached:

(1) A damage accumulation and failure criterion based on the PFC was proposed. It accounts for damage pathways and the number of cracks.

(2) Under horizontal seismic waves, cracks formed at the maximum absolute amplitude of the waveform and propagated through the dam in 0.82 s. The cracks began at the downstream toe, propagated diagonally downward, and penetrated the dam's upstream face. The dam failed due to through-cracks resulting from significant horizontal displacement differences. The horizontal displacement difference exhibited two peaks: one before crack initiation and another after crack propagation through the dam.

(3) Under vertical seismic waves, a crack penetrated the dam at 0.018 s. It originated from the downstream slope break and propagated diagonally downward, penetrating the dam's upstream face. This crack occurred due to a vertical displacement difference between the upstream and downstream faces, resulting in dam failure.

(4) The greater the inertial force of horizontal seismic waves, the faster the rate of damage accumulation and failure, and the earlier the crack formed. The effect of the inertial force on the dam's failure mode was pronounced: the smaller the inertial force, the more damage cracks formed.

(5) The inertial force of the vertical seismic waves had a negligible effect on the damage accumulation rate, crack initiation time, or failure mode.

 doi:10.20944/preprints202603.1989.v1

Author Contributions: Conceptualization, B.S., S.C., K.S. and Z.S.; methodology, B.S.; software, B.S.; validation, B.S. and S.C.; formal Analysis, B.S., Z.S., W.L., Y.H. and X.Q.; investigation, K.S.; resources, B.S., S.C., K.S. and Z.S.; data curation, B.S. and X.Q.; writing—original draft preparation, B.S.; writing—review and editing, B.S., S.C., K.S., Z.S., W.L., Y.H. and X.Q.; supervision, S.C., K.S., Z.S. and W.L.; project administration, B.S. and S.C.; funding acquisition, B.S., S.C., Z.S., W.L. and Y.H. All authors have read and agreed to the published version of the manuscript.

Funding: This research work was funded by the National Natural Science Foundation of China (Grant No. 52404134), the Natural Science Foundation of Shandong Provincial (ZR2023QE087), the Scientific Research Projects of Colleges and Universities in Anhui Province (2024AH050315, 2023AH051841); the Talent Project of Anhui Science and Technology University ((JZYJ202202, JZYJ202102), the Fundamental Research Funds for the Universities of Henan Province (NSFRF220423), the opening project of Henan Key Laboratory of Underground Engineering and Disaster Prevention (KFKT2023-05).

Institutional Review Board Statement: Not applicable.

Informed Consent Statement: Not applicable.

Data Availability Statement: Not applicable.

Conflicts of Interest: The authors declare no conflict of interest. The funders had no role in the design of the study; in the collection, analyses, or interpretation of data; in the writing of the manuscript, and in the decision to publish the results..

References

1. Shu,Y.; Wang,G.; Lu,W.; Chen,M.; Lv,L.; Chen,Y. Damage characteristics and failure modes of concrete gravity dams subjected to penetration and explosion. *Eng. Fail. Anal.* **2022**, 134, 106030. http://doi.org/10.1016/j.engfailanal.2022.106030.
2. Cao,M.; Han,B.; Kong,X.; Fang,Q.; Xie,H.; Lei,Y.; Hu,J.; Zhang,X. Failure mode of concrete gravity dams subjected to internal explosion: centrifuge test and numerical simulation. *Int. J. Impact Eng.* **2026**, 208, 105517. http://doi.org/10.1016/j.ijimpeng.2025.105517.
3. Wang,F.; Tan,Y.; Liu,Y.; Song,Z.; Liu,X.; Li,C. Response analysis of concrete gravity dams based on direct numerical simulation method for wave propagation in reservoir water. *Soil Dyn. Earthq. Eng.* **2026**, 204, 110206. http://doi.org/10.1016/j.soildyn.2026.110206.
4. Gao,Z.; Wang,G.; Lu,W.; Liu,S.; Pan,X.; Qi,Z. A new impact factor considering structural morphology for concrete gravity dams subjected to underwater non-contact explosion. *Eng. Struct.* **2025**, 341, 120826. http://doi.org/10.1016/j.engstruct.2025.120826.
5. Cao,K.; Fu,Q.; Zhang,J.; Huang,J.; Zhao,Y. Evaluation of the explosion-proof effect and damage prediction of a gravity dam reinforced with a composite corrugated steel–concrete slab structure under different factors. *Constr. Build. Mater.* **2025**, 479, 141479. http://doi.org/10.1016/j.conbuildmat.2025.141479.
6. Chopra,A.; Chakrabarti,P. The Koyna earthquake and the damage to Koyna Dam. B. Seismol. Soc. Am. **1973**, 63(2), 381-397. http://doi.org/10.1785/BSSA0630020381.
7. Wieland,M.; Matsumoto,N.; Landon-Jones,I.; Babbitt,D. Inspection of dams after earthquakes. *Chin. J. Geotech. Eng.* **2008**, 30(11), 1661-1668. https://kns.cnki.net/kcms2/article/abstract?v=FCWB7knoBeSoV04VCbsOCHfG9t_C8wMBWjEg8F2GcyPgQ7MsyhAEpGEoV4KrO4Ih0jxATiD9ZL2qeuGNUxSb-RjXH6JXD0perPYzY8fdVDE-R01fvFC8oEfrqJBbdrxy8tOTkA35SnYvsF--LXuMil5WdMLW9Q9cNP2R7MAmFsxWJflKo2sH1gDW5K2k6Iv_&uniplatform=NZKPT.
8. Kianoush,M.; Ghaemmaghami,A. The effect of earthquake frequency content on the seismic behavior of concrete rectangular liquid tanks using the finite element method incorporating soil–structure interaction. *Eng. Struct.* **2011**, 33(7), 2186-2200. http://doi.org/10.1016/j.engstruct.2011.03.009.
9. Xu,Q.; Xu,S.; Chen,J.; Li,J. Dimensionless analysis of pulse-like effects on the seismic behavior of a dam based on wavelet-decomposed near-fault ground motions. *Structures* **2021**, 33, 2003-2018. http://doi.org/10.1016/j.istruc.2021.05.069.

 doi:10.20944/preprints202603.1989.v1

10. Siva,P.; Mahesh,M.; Raj,K. Critical crack lengths of concrete gravity dam by using fracture mechanics. *Mater. Today: Proc.* **2021**, 38, 3149-3159. http://doi.org/10.1016/j.matpr.2020.09.505.
11. Sabbagh-Yazdi,S.; Farhoud,A.; Mohammadi,A.; Yazdinasabkarani,E. Earthquake damage estimation of the Koyna concrete gravity dam using explicit GFVM model considering fluid–structure interaction. *Math. Comput. Simul.* **2022**, 195, 151-170. http://doi.org/10.1016/j.matcom.2022.01.002.
12. Huang,X.; Kong,X.; Hu,J.; Fang,Q. Failure modes of concrete gravity dam subjected to near-field underwater explosion: Centrifuge test and numerical simulation. *Eng. Fail. Anal.* **2022**, 137, 106243. http://doi.org/10.1016/j.engfailanal.2022.106243.
13. Haghani,M.; Navayi,N.; Ahmadi,M.; Vaseghi,A. Combining XFEM and time integration by α-method for seismic analysis of dam-foundation-reservoir. *Theor. Appl. Fract. Mech.* **2020**, 109, 102752. http://doi.org/10.1016/j.tafmec.2020.102752.
14. Adib,A.; Moradloo,A. Seismic damage prediction in concrete gravity dams using a new framework based on Machine learning. *Int. J. Solids Struct.* **2026**, 113928. http://doi.org/10.1016/j.ijsolstr.2026.113928.
15. Shiyam,S.; Shrimali,M.; Bharti,S.; Datta,T. Effect of foundation flexibility on the seismic damage of concrete gravity dams in aftershocks. *Structures* **2025**, 80, 109948. http://doi.org/10.1016/j.istruc.2025.109948.
16. Khoshnafas,M.; Mirhosseini,M.; Lajevardi,S.; Zeighami,E. Effect of foundation stiffness on the fragility curves of a concrete gravity dam under far-field ground motions. *Results in Engineering* **2024**, 24, 102962. http://doi.org/10.1016/j.rineng.2024.102962.
17. Soysal,Berat.; Arici,Y. The use of discrete element models for the seismic assessment of concrete gravity dams. *Structures* **2024**, 70, 107831. http://doi.org/10.1016/j.istruc.2024.107831.
18. Zhong,H.; Wang,N.; Lin,G. Seismic response of concrete gravity dam reinforced with FRP sheets on dam surface. *Water Sci. Eng.* **2013**, 6(4), 409-422. http://doi.org/10.3882/j.issn.1674-2370.2013.04.005.
19. Guanglun,W.; Pekau,O.; Chuhan,Z.; Shaomin,W. Seismic fracture analysis of concrete gravity dams based on nonlinear fracture mechanics. *Eng. Fract. Mech.* **2000**, 65(1), 67-87. http://doi.org/10.1016/S0013-7944(99)00104-6.
20. Lee,J.; Fenves,G. A plastic-damage concrete model for earthquake analysis of dams. E*arthq. Eng. Struct. Dyn.* **1998**, 27(9), 937-956. http://doi.org/10.1002/(SICI)1096-9845(199809)27:9<937::AID-EQE764>3.0.CO;2-5.
21. Nariman,N.; Nariman,N.; Lahmer,T.; Lahmer,T.; Karampour,P.; Karampour, P. Uncertainty quantification of stability and damage detection parameters of coupled hydrodynamic-ground motion in concrete gravity dams. *Front. Struct. Civ. Eng.* **2019**, 13(2), 303-323. http://doi.org/10.1007/s11709-018-0462-x.
22. Sun,B.; Chen,R.; Ping,Y.; Zhu,Z.; Wu,N. Study on Axial Tensile Strain Rate Effect on Concrete Based on Experimental Investigation and Numerical Simulation. *Materials* **2022**, 15(15), 5164. http://doi.org/10.3390/ma15155164.
23. Sun,B.; Chen,R.; Ping,Y.; Zhu,Z.; Wu,Nan; He,Y. Dynamic Response of Rock-like Materials Based on SHPB Pulse Waveform Characteristics. *Materials* **2022**, 15(1), 210. http://doi.org/10.3390/ma15010210.
24. Sun,B.; Chang,S.; Ma,L.; Lu,W.; He,Y.; Shi,Z. Sensitivity analysis of rock dynamic response based on a multi-scale parameter model. *Phys. Fluids* **2025**, 37(9), 97110. http://doi.org/10.1063/5.0285159.